Harnessing Geometric Frustration to Form Band Gaps in Acoustic Channel Lattices

Pai Wang,[1] Yue Zheng,[2] Matheus C. Fernandes,[1] Yushen Sun,[3] Kai Xu,[4] Sijie Sun,[1,3] Sung Hoon Kang,[5]
Vincent Tournat,[1,6,*] and Katia Bertoldi[1,7,†]

[1]*Harvard John A. Paulson School of Engineering and Applied Science, Harvard University, Cambridge,
Massachusetts 02138, USA*
[2]*Jacobs School of Engineering, University of California, San Diego, California 92093, USA*
[3]*Tsinghua University, Beijing 100084, China*
[4]*Peking University Shenzhen Graduate School, Shenzhen 518055, China*
[5]*Department of Mechanical Engineering, Johns Hopkins University, Baltimore, Maryland 21218, USA*
[6]*LAUM, CNRS, Université du Maine, Avenue O. Messiaen, 72085 Le Mans, France*
[7]*Kavli Institute, Harvard University, Cambridge, Massachusetts 02138, USA*
(Received 15 August 2016; published 21 February 2017)

We demonstrate both numerically and experimentally that geometric frustration in two-dimensional periodic acoustic networks consisting of arrays of narrow air channels can be harnessed to form band gaps (ranges of frequency in which the waves cannot propagate in any direction through the system). While resonant standing wave modes and interferences are ubiquitous in all the analyzed network geometries, we show that they give rise to band gaps only in the geometrically frustrated ones (i.e., those comprising of triangles and pentagons). Our results not only reveal a new mechanism based on geometric frustration to suppress the propagation of pressure waves in specific frequency ranges but also open avenues for the design of a new generation of smart systems that control and manipulate sound and vibrations.

Geometric frustration arises when interactions between the degrees of freedom in a lattice are incompatible with the underlying geometry [1,2]. This phenomenon plays an important role in many natural and synthetic systems, including water ice [3], spin ice [4–6], colloids [7–9], liquid crystals [10], and proteins [11,12]. Surprisingly, despite the fact that geometric frustration is scale-free, it has been primarily studied at the microscale [2], and only very recently has the rich behavior of macroscopic frustrated systems been explored [13,14]. Here, we investigate both numerically and experimentally the effect of geometric frustration on the propagation of sound waves in 2D macroscopic acoustic networks.

We focus on periodic arrays of narrow air channels of length L and note that a propagating mode with wavelength $\lambda = 2L$ [see Fig. 1(a)] can be perfectly accommodated by a rhombic lattice, independent of the angle θ between the channels [see Figs. 1(b) and 1(c) for $\theta = \pi/2$—the well-known square lattice—and $\theta = \pi/3$, respectively]. However, when we form a triangular lattice by adding an additional channel to a rhombic network with $\theta = \pi/3$, such a mode is no longer supported [see Fig. 1(d)], and the system becomes frustrated. This leads us to investigate the following question: How does geometric frustration affect the dynamic response of a periodic acoustic network?

Our combined numerical and experimental results demonstrate that, while a rhombic network transmits acoustic waves of any frequency, a triangular network shows full Bragg-type sonic band gaps. While sonic Bragg-type band gaps have been previously demonstrated in ordered arrays

of solid inclusions in air [15–19], the necessary conditions for destructive interferences leading to their opening are usually unknown in 2D systems, and their prediction always required detailed numerical simulations. Nonlocal homogenization theories, e.g., [20], could, in principle, be used to calculate the band gaps, but they would require numerical calculations of a similar level of complexity. Here, we identify a new strategy based on geometric frustration to form full Bragg-type band gaps at the desired
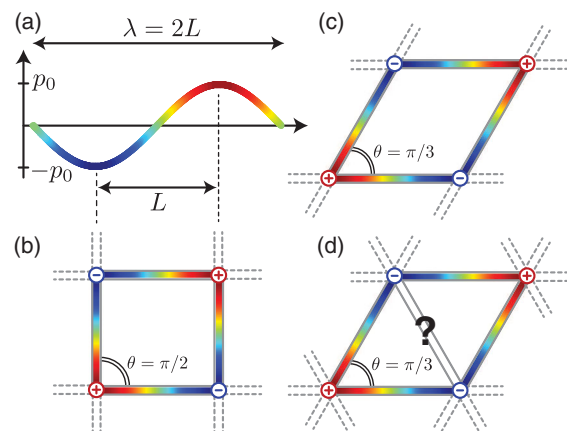

FIG. 1. Geometric frustration in acoustic networks: (a) A propagating mode with a wavelength twice that of a single channel length (i.e., $\lambda = 2L$) can be supported by a rhombic network with (b) $\theta = \pi/2$ and (c) $\theta = \pi/3$ but cannot be supported by (d) the triangular network, causing the system to become frustrated.

frequencies. Remarkably, we derive robust and simple rules to exactly predict the location of the band gaps solely as a function of the arrangement of the propagating media. This provides a powerful tool for the design of systems capable of precisely controlling the propagation of sound.

In order to analyze the effect of geometric frustration on the propagation of sound waves, we first calculate the dispersion relations for periodic acoustic networks composed of narrow air channels of length L and cross-sectional width D, with $D \ll L$. Assuming that in any channel $\lambda > 2D$ and the viscous and thermal boundary layer thicknesses are small compared to D, we used the 1D wave equation [21] to describe the free vibrations of the enclosed air column. Furthermore, we determine the dispersion relations of a periodic network both analytically [22] and numerically (more details on the analysis are provided in Supplemental Material [23], and the finite element (FE) code implemented in MATLAB is available online [24]).

In Fig. 2, we show the acoustic dispersion curves for the square and triangular networks in terms of the normalized frequency $\Omega = \omega L/(2\pi c) = L/\lambda$, where ω denotes the angular frequency of the propagating pressure wave and $c = 343.2$ m/s is the speed of sound in air. Both analytical (continuous lines) and numerical (circular markers) results are reported and show perfect agreement. First, we note that both band structures are periodic in Ω and are characterized by equally spaced flat bands located at $\Omega = n/2$ (n being an integer, $n = 1, 2, 3, \ldots$). This is a clear signature of the expected resonant modes with wavelengths $\lambda_n = 2L/n$ localized in the individual air channels. These modes (which are not captured by our analytical model, as we considered only propagating waves in the calculations) are characterized by zero pressure at both ends of each channel. As such, they are geometrically compatible with both the square and triangular networks (as well as any other equilateral lattice geometry), since continuity conditions at the junctions can always be satisfied.

Second, and more importantly, the dispersion curves reported in Fig. 2 also indicate that, while the square lattice transmits acoustic waves of any frequency, full band gaps exist in the triangular network, as highlighted by the shaded areas in Fig. 2(b). These band gaps open around the odd-numbered resonant modes (i.e., $n = 1, 3, 5, \ldots$), the first one (i.e., $n = 1$) corresponding to $\lambda = 2L$. Note that these odd-numbered modes introduce a specific coupling condition between the ends of each air channel: The pressure field phasor is opposite for neighboring junctions. Therefore, at these specific frequencies, the acoustic triangular network behaves as the frustrated antiferromagnetic triangle, where each spin cannot be antialigned with all its neighbors [1,2]. More specifically, in the considered acoustic lattice, the phasor of the pressure field plays the role of the spin, while the opposite phasor between the two ends of each individual channel occurring at $\Omega = n/2$ introduces conditions analogous to the antiferromagnetic coupling. However, differently from the case of antiferromagnetic interactions, in our acoustic networks the coupling between neighboring junctions depends on the wave frequency, so that geometric frustration arises only at specific values of Ω [25].

We find that all lattices showing geometric frustration under antiferromagnetic spin coupling exhibit full acoustic band gaps in their dispersion spectrum, while those that can accommodate such coupling and are not frustrated do not (see Fig. S6 in Ref. [23]). Furthermore, while the results presented in Fig. 2 are for ideal acoustic networks made of 1D channels, we have also investigated the effect of the finite width D of the tubes. The numerical results reported in Fig. S7 [23] for networks formed by channels with different L/D ratios indicate that the dynamic response of the system is not significantly affected by the finite width of the channels. In fact, the triangular network is still characterized by full band gaps around the odd-numbered resonant modes even for $L/D = 10$.

Having demonstrated that geometric frustration can be exploited to form band gaps in acoustic networks, we now shed light on the mechanism leading to their opening. To this extent, we consider a rhombic lattice with $\theta = \pi/3$ and
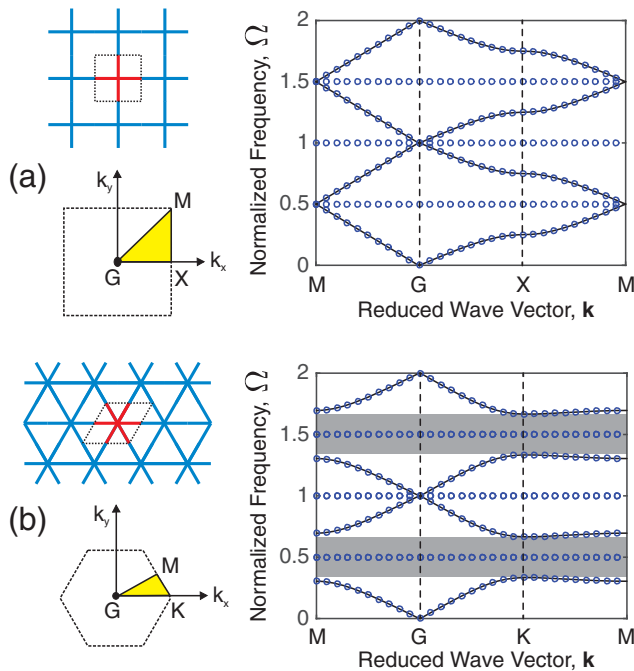

FIG. 2. Dispersion relations of acoustic networks comprising a periodic array of air channels: (a) square lattice and (b) triangular lattice. Continuous lines and circular markers correspond to analytical and numerical (finite element) results, respectively. The shaded regions in (b) highlight the full band gaps induced by geometric frustration. Lattice configurations, unit cells (highlighted in red), and irreducible Brillouin zones are shown on the left.

$L/D = 100$ and analyze numerically the effect of a channel of width d added along its short diagonal (see the schematics in Fig. 3). In Fig. 3, we report the dispersion curves along the GM direction for different values of d/D ranging from 0 (rhombic lattice) to 1 (triangular lattice). Our results reveal that, as soon as the coupling induced by the additional channel of width $d \ll D$ is present, a band gap opens at point M. Moreover, as d/D increases, the width of the band gap monotonically raises and approaches that of the triangular lattice. Mode shapes at the cutoff frequency are represented in Fig. 3 for $d/D = 0.0$ (rhombic network), $d/D = 0.2$, and $d/D = 1.0$ (triangular network). They indicate that the additional diagonal channel completely changes the pressure distribution, as that of the rhombic lattice ($d/D = 0$) is no further compatible with the underlying geometry when the diagonal channel is added. The coupling introduced by the additional channel results in new interferences (coupling) that modify the mode shapes and frequencies of the periodic networks and eventually lead to the opening of full band gaps.

The results shown in Fig. 3 indicate that the band gaps are of the Bragg type, as they can be interpreted as the result of the destructive interferences of waves propagating in the individual channels and scattered at each junction of the lattice with a specific amplitude and phase [26,27]. An analysis of the dispersion curves also reveals that inside the band gap $\mathrm{Re}(\mathbf{k}) = \pi$ and $\mathrm{Im}(\mathbf{k})$ is rounded and symmetric [see Fig. S5(b) of Ref. [23]], two features that are consistent with Bragg band gaps. As a consequence, and also due to the fact that there is no local resonances in the studied lattices, the band gaps are not due to hybridization or to the coupling of local resonators (a coupling such as tunneling or analogous to the tight binding in crystals) [28,29].
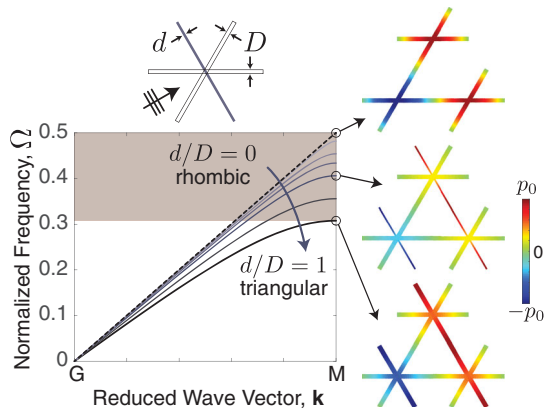
Finally, we characterize both numerically and experimentally the dynamic response of acoustic networks of a finite size. We start by conducting a numerical steady-state analysis to calculate the transmission through finite-size networks comprising 6×6 unit cells made of 2D channels with $L/D = 20$, in accordance with the tested sample configurations. In these simulations, a harmonic input pressure p^{in} is applied at the end of the central channel on the left edge of the model. In Fig. 4, we report the steady-state pressure fields obtained for the square and triangular networks at $\Omega = 0.45$ (in the gap induced by geometric frustration in the triangular network) and $\Omega = 0.95$ (in the vicinity of the second resonant frequency of a single channel). The results show that in the triangular network at $\Omega = 0.45$ the acoustic energy is completely localized near the excitation site and no signal is transmitted to the opposite end of the lattice [Fig. 4(c)]—a clear indication of a full band gap. On the other hand, in all other cases the acoustic waves are found to propagate across the finite networks, even in the presence of partial band gaps [Figs. 4(a), 4(b), and 4(d)].

To validate these predictions, we fabricated samples of the square and triangular acoustic networks comprising 6×6 unit cells [Figs. 5(a) and 5(b)]. The individual air channels have length $L = 40$ mm and a square cross section of 2×2 mm (so that $L/D = 20$ and $\Omega = 0.5$ corresponds to a frequency of 4 kHz) and were engraved into an acrylic plate of thickness 8 mm by milling with computerized numerical control. A flat acrylic plate was then glued on the top of the etched plate to cover the air channels. During all the experiments, the sample was surrounded with sound-absorbing foams to minimize the effect of the ambient noise and the room reverberation. Moreover, an open channel on one of the edges of the
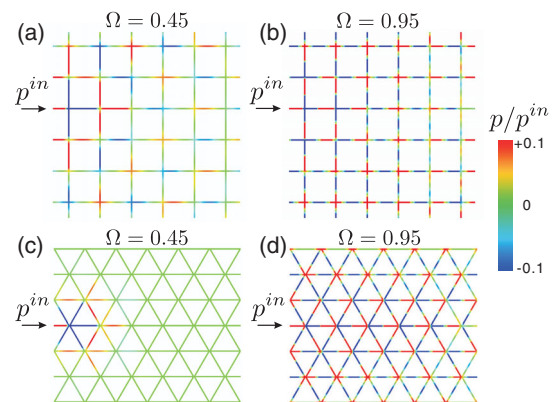

FIG. 3. Dynamic response of a rhombic lattice with an additional channel of width d along the short diagonal. Dispersion curves along the GM direction are plotted for different values of channel width ratios d/D. Mode shapes at the M point are shown for three unit cells characterized by $d/D = 0$ (rhombic lattice), $d/D = 0.2$, and $d/D = 1$ (triangular lattice). Note that for visualization purposes the channel width D is increased to $L/D = 20$ (while in the calculations we used $L/D = 100$).

FIG. 4. Pressure field distribution in finite-sized acoustic networks comprising 6×6 unit cells: (a) square lattice at $\Omega = 0.45$, (b) square lattice at $\Omega = 0.95$, (c) triangular lattice at $\Omega = 0.45$, and (d) triangular lattice at $\Omega = 0.95$. The color indicates the pressure amplitude normalized by the input signal amplitude (p^{in}).
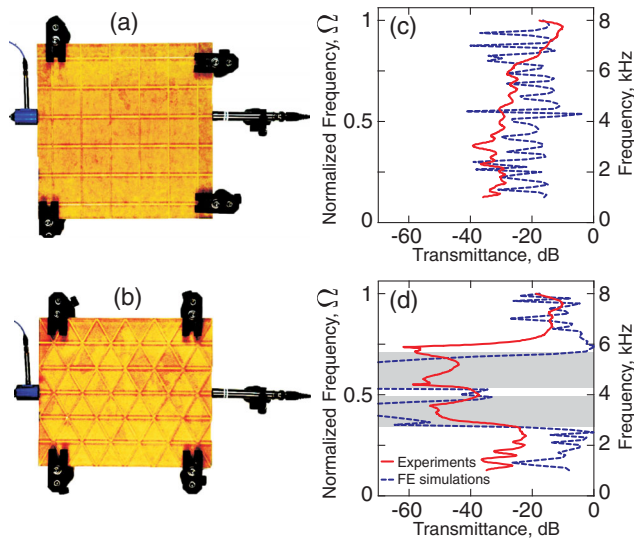
FIG. 5. Transmittance of finite-sized networks: fabricated samples with the (a) square and (b) triangular networks. The input chamber is connected to the left edge of the samples, while the microphone to measure the amplitude of the transmitted sound waves is attached to the right edge. The frequency-dependent transmittances for the samples are shown in (c) and (d) for the square and triangular network, respectively. Both experimental (continuous red line) and numerical (dashed blue line) results are shown. The gray regions in (d) highlight the full band gap as predicted for the corresponding infinite structure [see Fig. 2(b)].

samples was connected to an input chamber containing an earphone (352C22, PCB Piezotronics) to excite a broadband white noise signal between 1 and 8 kHz and a microphone to measure the amplitude of the generated sound waves p^{in}. Another microphone was then placed at an air channel opening on the opposite side of the sample to detect the transmitted signal p^{out}, and the acoustic transmittance is calculated as the ratio p^{out}/p^{in}. Note that, since the tested samples are of a finite size and the source excites a single channel, the waves are generated in several directions and then scattered in many others. As such, in our experiments we test not only x-direction transmission but multiple-direction transmission. This is confirmed by the fact that directional band gaps in the x direction do not lead to a drop in the experimental transmittance spectrum.

The continuous red lines in Figs. 5(c) and 5(d) show the experimentally measured transmittance for the square and triangular samples, respectively, while the blue dashed lines correspond to the transmittance as predicted by steady-state FE simulations. The latter are carried out on 2D models with the exact geometries of the samples and with absorbing conditions at the sample edges. However, we found that transmittance gaps and their positions are robust features and are not affected by either the boundary condition type or the macroscopic shape of the samples. First, we note that

the transmittance for the square lattice does not show regions of significant attenuation and fluctuates around −30 dB for experimental data and around −20 dB for numerical results. Such a low baseline value can be mainly attributed to the radiation of acoustic energy through the channel openings on the edges, while the 10 dB difference between experimental and numerical results can be attributed to the dissipation in the viscous and thermal boundary layers [30,31], an effect which is more pronounced at the low frequencies and is not accounted for in the FE simulations. In contrast, for the triangular network, a significant drop (up to ∼ − 60 dB) in the transmittance is observed between 2.5 and 6 kHz (i.e., for Ω between 0.3 and 0.7), confirming the existence of the full band gap induced by geometric frustration. Note that our experiments also capture the narrow transmission band at $\Omega \simeq 0.5$, which is predicted by the dispersion relations for a triangular lattice with $L/D = 20$ (see Fig. S7 of Ref. [23]).

In summary, we demonstrated both numerically and experimentally that geometric frustration in networks of channels can be exploited to control the propagation of sound waves. Particularly, we found that in acoustic networks comprising frustrated units (such as triangles and pentagons) full Bragg-type band gaps emerge in the vicinity of the odd-numbered resonant frequencies of the individual channels, as these introduce conditions analogous to the antiferromagnetic coupling in spin lattices. Therefore, our study points to an effective and powerful rule to construct acoustic structures whose band gaps can be predicted *a priori*, purely based on the arrangement of the channels in the network. While the necessary conditions for destructive interferences leading to the opening of a full Bragg band gap are usually unknown in 2D systems, we found that geometric frustration results in gaps at specific and predictable frequencies, which depends only on the length of the tubes.

Given the broad range of applications recently demonstrated for systems with acoustic band gaps, including wave guiding [32,33], frequency modulation [34,35], noise reduction [36], and acoustic imaging [37–39], we expect geometrically frustrated acoustic networks to play an important role in the design of the next generation of materials and devices that control the propagation of sound. These systems could be made more compact by coiling up space [40]. Furthermore, exotic functionalities could be achieved with more elaborate designs which incorporate local resonators, additional coupling channels, and fractal structures. For instance, our strategy could provide a tool for the design of acoustic media with an effective zero index [41,42] or topologically protected edge modes [43,44].

―――――――――

*Corresponding author.
vincent.tournat@univ-lemans.fr
†Corresponding author.
bertoldi@seas.harvard.edu

[1] J.-F. Sadoc and R. Mosseri, *Geometrical Frustration* (Cambridge University Press, Cambridge, England, 2006).

[2] R. Moessner and A. P. Ramirez, Phys. Today **59**, No. 2, 24 (2006).

[3] L. Pauling, J. Am. Chem. Soc. **57**, 2680 (1935).

[4] P. E. Lammert, X. Ke, J. Li, C. Nisoli, D. M. Garand, V. H. Crespi, and P. Schiffer, Nat. Phys. **6**, 786 (2010).

[5] J. P. Morgan, A. Stein, S. Langridge, and C. H. Marrows, Nat. Phys. **7**, 75 (2011).

[6] A. Farhan, P. Derlet, A. Kleibert, A. Balan, R. Chopdekar, M. Wyss, L. Anghinolfi, F. Nolting, and L. Heyderman, Nat. Phys. **9**, 375 (2013).

[7] Y. Han, Y. Shokef, A. M. Alsayed, P. Yunker, T. C. Lubensky, and A. G. Yodh, Nature (London) **456**, 898 (2008).

[8] P. Yunker, Z. Zhang, and A. G. Yodh, Phys. Rev. Lett. **104**, 015701 (2010).

[9] Y. Shokef, Y. Han, A. Souslov, A. Yodh, and T. C. Lubensky, Soft Matter **9**, 6565 (2013).

[10] X. Zeng, R. Kieffer, B. Glettner, C. Nurnberger, F. Liu, K. Pelz, M. Prehm, U. Baumeister, H. Hahn, H. Lang, G. A. Gehring, C. H. M. Weber, J. K. Hobbs, C. Tschierske, and G. Ungar, Science **331**, 1302 (2011).

[11] J. D. Bryngelson and P. G. Wolynes, Proc. Natl. Acad. Sci. U.S.A. **84**, 7524 (1987).

[12] B. G. Wensley, S. Batey, F. A. Bone, Z. M. Chan, N. R. Tumelty, A. Steward, L. G. Kwa, A. Borgia, and J. Clarke, Nature (London) **463**, 685 (2010).

[13] P. Mellado, A. Concha, and L. Mahadevan, Phys. Rev. Lett. **109**, 257203 (2012).

[14] S. H. Kang, S. Shan, A. Košmrlj, W. L. Noorduin, S. Shian, J. C. Weaver, D. R. Clarke, and K. Bertoldi, Phys. Rev. Lett. **112**, 098701 (2014).

[15] M. Sigalas and E. Economou, Europhys. Lett. **36**, 241 (1996).

[16] M. S. Kushwaha, Appl. Phys. Lett. **70**, 3218 (1997).

[17] R. Martinezsala, J. Sancho, J. Sánchez, V. Gómez, J. Llinares, and F. Meseguer, Nature (London) **378**, 241 (1995).

[18] J. V. Sánchez-Pérez, D. Caballero, R. Martinez-Sala, C. Rubio, J. Sánchez-Dehesa, F. Meseguer, J. Llinares, and F. Gálvez, Phys. Rev. Lett. **80**, 5325 (1998).

[19] W. Robertson and J. Rudy III, J. Acoust. Soc. Am. **104**, 694 (1998).

[20] D. Lafarge and N. Nemati, Wave Motion **50**, 1016 (2013).

[21] P. M. Morse and K. U. Ingard, *Theoretical Acoustics* (Princeton University, Princeton, NJ, 1968).

[22] C. Depollier, J. Kergomard, and J. C. Lesueur, J. Sound Vib. **142**, 153 (1990).

[23] See Supplemental Material at http://link.aps.org/supplemental/10.1103/PhysRevLett.118.084302 for additional results and detailed derivations and calculation procedures, which includes references.

[24] For the MATLAB code implemented to calculate the dispersion relations of acoustic networks comprising a periodic arrays of narrow air channels, see files at http://link.aps.org/supplemental/10.1103/PhysRevLett.118.084302.

[25] Note that in the triangular network no band gap opens in correspondence of the even-numbered resonant modes (i.e., $n = 2, 4, 6, \ldots$), as these modes are characterized by identical pressure field phases at the two ends of each individual channel and therefore can be supported by any acoustic network.

[26] The long-wavelength scattering by a junction of N identical channels can be obtained analytically. Interestingly, it does not vanish at a very long wavelength and is strongly anisotropic due to the junction geometry, which makes this scatterer different from an inclusion in a host medium.

[27] M. Molerón, G. Dubois, O. Richoux, S. Félix, and V. Pagneux, Acta Acust. Acust. **100**, 391 (2014).

[28] C. Croënne, E. J. S. Lee, H. Hu, and J. H. Page, AIP Adv. **1**, 041401 (2011).

[29] F. Lemoult, N. Kaina, M. Fink, and G. Lerosey, Nat. Phys. **9**, 55 (2013).

[30] G. P. Ward, R. K. Lovelock, A. R. J. Murray, A. P. Hibbins, J. R. Sambles, and J. D. Smith, Phys. Rev. Lett. **115**, 044302 (2015).

[31] M. Bruneau and T. Scelo, *Fundamentals of Acoustics* (Wiley-ISTE, New York, 2006).

[32] M. Ruzzene, F. Scarpa, and F. Soranna, Smart Mater. Struct. **12**, 363 (2003).

[33] X. Zhang and Z. Liu, Appl. Phys. Lett. **85**, 341 (2004).

[34] M. Kafesaki, M. M. Sigalas, and N. Garcia, Phys. Rev. Lett. **85**, 4044 (2000).

[35] Y. Pennec, B. Djafari-Rouhani, J. O. Vasseur, A. Khelif, and P. A. Deymier, Phys. Rev. E **69**, 046608 (2004).

[36] J. Mei, G. Ma, M. Yang, Z. Yang, W. Wen, and P. Sheng, Nat. Commun. **3**, 756 (2012).

[37] F. Liu, F. Cai, S. Peng, R. Hao, M. Ke, and Z. Liu, Phys. Rev. E **80**, 026603 (2009).

[38] J. Zhu, J. Christensen, J. Jung, L. Martin-Moreno, X. Yin, L. Fok, X. Zhang, and F. Garcia-Vidal, Nat. Phys. **7**, 52 (2011).

[39] M. Molerón and C. Daraio, Nat. Commun. **6**, 8037 (2015).

[40] Z. Liang and J. Li, Physical review and Physical review letters index **108**, 114301 (2012).

[41] L.-Y. Zheng, Y. Wu, X. Ni, Z.-G. Chen, M.-H. Lu, and Y.-F. Chen, Appl. Phys. Lett. **104**, 161904 (2014).

[42] F. Liu, X. Huang, and C. T. Chan, Appl. Phys. Lett. **100**, 071911 (2012).

[43] T. C. Lubensky, C. L. Kane, A. Xiaoming Mao, Souslov, and K. Sun, Rep. Prog. Phys. **78**, 073901 (2015).

[44] V. Vitelli, Proc. Natl. Acad. Sci. U.S.A. **109**, 12266 (2012).

Supplemental Material to
Harnessing Geometric Frustration to Form Band Gaps in Acoustic Networks

Pai Wang,[1] Yue Zheng,[2] Matheus C. Fernandes,[1] Yushen Sun,[3] Kai Xu,[4]

Sijie Sun,[1] Sung Hoon Kang,[5] Vincent Tournat,[1,6] and Katia Bertoldi[1,7]

[1]*Harvard John A. Paulson School of Engineering and Applied Science, Harvard University, Cambridge, MA 02138*
[2]*Jacobs School of Engineering, University of California, San Diego, CA 92093*
[3]*Tsinghua University, Beijing, China*
[4]*Peking University Shenzhen Graduate School, Shenzhen, China*
[5]*Department of Mechanical Engineering, Johns Hopkins University, Baltimore, MD 21218*
[6]*LAUM, CNRS, Université du Maine, Av. O. Messiaen, 72085 Le Mans, France*
[7]*Kavli Institute, Harvard University, Cambridge, MA 02138*

ANALYTICAL CALCULATION OF DISPERSION RELATIONS FOR PERIODIC ACOUSTIC NETWORKS

To analytically obtain the dispersion relations for periodic acoustic networks composed of identical narrow air channels of length L that support only a planar mode, we start by focusing on an individual tube (see Fig. S4(a)). Using transmission line theory [1, 2], it is possible to express the acoustic particle velocity u_0 at one end of the channel ($x = 0$) as a function of the pressures p_0, p_L at both ends ($x = 0$ and L) of the channel as,

$$u_0 = Y p_0 + Y' p_L, \tag{S1}$$

where

$$Y = -\frac{\imath}{Z_c} \cot(kL), \qquad \text{and} \qquad Y' = \frac{\imath}{Z_c} \sin^{-1}(kL). \tag{S2}$$

Here, $Z_c = \rho_0 c_0 / D$ is the characteristic impedance of the air channel, ρ_0 is the air density, $c_0 = 343$ m/s is the acoustic wave velocity, L is the channel length, D is the channel width, $k = \omega/c_0$ is the wavenumber, ω is the cyclic frequency, and $\imath = \sqrt{-1}$ (time convention $e^{\imath \omega t}$).

The response of the network of channels can then be constructed by enforcing acoustic particle velocity flow conservation at each junctions where N tubes with the same width D are connected (see Fig. S4(b)),

$$\sum_{i=1}^{N} u_i = 0. \tag{S3}$$

Substitution of Eq. (S1) into Eq. (S3) yields

$$\sum_{i=1}^{N} (Y p + Y' p_i) = 0, \tag{S4}$$

where p is the pressure at the considered junction and p_i the pressure at the other end of the i-th tube connected to this junction. Since all the tubes are identical (i.e. of the same length L and same width D) and $-Y/Y' = \cos(kL)$, Eq. (S4) can be rewritten as

$$N p \cos(2\pi\Omega) - \sum_{i=1}^{N} p_i = 0, \tag{S5}$$

where $\Omega = kL/(2\pi)$ is the normalized frequency.

Eq. (S5) fully describes the behavior of a junction as it provides the local pressure p as a function of the pressures p_i at the surrounding junctions for a given frequency. Therefore, it forms the basis to obtain the dispersion relations for a network of channels.
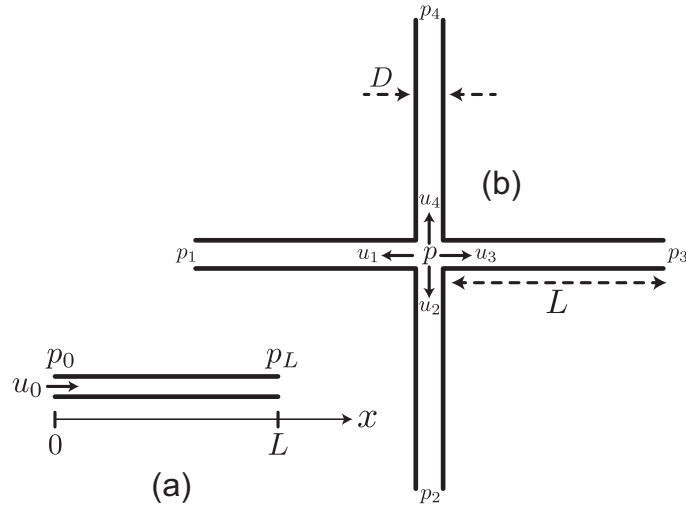
FIG. S1: (a) Definition of the field quantities in a portion of tube of length L. (b) Definition of the field quantities at a junction. The u_i are the outgoing acoustic particle velocities for each branch i, and p_i are the pressures at the end of branches i.

Dispersion relation for the square lattice ($N = 4$)

For a square lattice we have $N = 4$, so that Eq. (S5) becomes

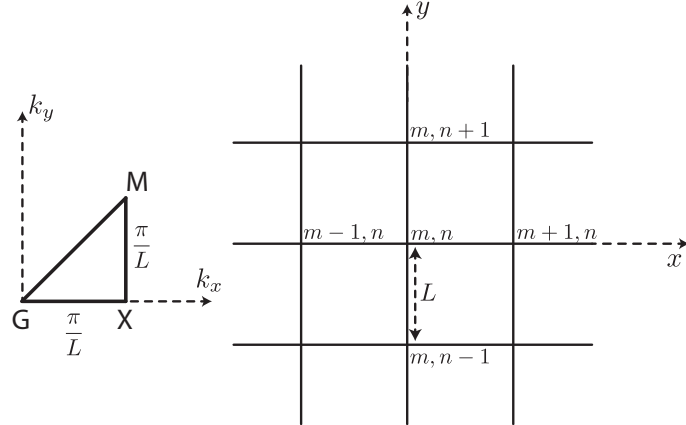$$4p\cos(2\pi\Omega) - \sum_{i=1}^{4} p_i = 0. \tag{S6}$$

FIG. S2: Geometrical configuration of the square lattice and Brillouin zone definition.

Focusing on the junction labelled with the indexes (m, n) in Fig. S2, Eq.(S6) can be rewritten as,

$$4p_{(m,n)}\cos(2\pi\Omega) - p_{(m,n-1)} - p_{(m,n+1)} - p_{(m-1,n)} - p_{(m+1,n)} = 0. \tag{S7}$$

Assuming periodicity and a solution in the form of a propagating wave $e^{-\imath k_x x - \imath k_y y}$, with k_x and k_y the coordinates of the wave vector $\mathbf{k}$, we find

$$4\cos(2\pi\Omega) - e^{\imath k_y L} - e^{-\imath k_y L} - e^{\imath k_x L} - e^{-\imath k_x L} = 0, \tag{S8}$$

which can be rewritten compactly as

$$4\cos(2\pi\Omega) - 2\cos(k_y L) - 2\cos(k_x L) = 0. \tag{S9}$$

Eq. (S9) is referred to as the dispersion equation of the square lattice and is solved for wave vectors $\mathbf{k} = [k_x, k_y]$ within the first Brillouin zone to obtain its band structure. More specifically, for the square acoustic network we solve the dispersion equation on the perimeter of the GMX contour shown in Fig. S2.

We start by noting that for the GX branch of the Brillouin zone, there is propagation only along the x-axis, so that $k_y = 0$. Therefore, Eq. (S9) simplifies to

$$4\cos(2\pi\Omega) - 2\cos(k^{GX}L) = 0, \tag{S10}$$

which can be easily solved to obtain the dispersion relation between the wavenumber k^{GX} and the frequency Ω,

$$k^{GX} = \frac{1}{L}\arccos(\cos(2\pi\Omega) - 1), \tag{S11}$$

or inverted as,

$$\Omega = \frac{\arccos[(\cos(k^{GX}L) + 1)/2]}{2\pi}, \qquad k^{GX} \in [0, \pi/L]. \tag{S12}$$

For the GM branch $k_y = k_x$, so that Eq. (S9) yields

$$k^{GM} = \arccos(\cos(2\pi\Omega))/L = 2\pi\Omega/L, \tag{S13}$$

which can be inverted to obtain the dispersion relation between frequency Ω and the wavenumber k^{GM}

$$\Omega = k^{GM}L/2\pi, \qquad k^{GM} \in [0, \pi/L]. \tag{S14}$$

Finally, for the XM branch $k_x = \pi$, so that Eq. (S9) yields

$$k^{XM}L = \arccos(2\cos(2\pi\Omega) + 1), \tag{S15}$$

which can be inverted to obtain the dispersion relation between frequency Ω and the wavenumber k^{GM}

$$\Omega = \frac{\arccos[\cos(k^{XM}L) - 1)/2)]}{2\pi}. \tag{S16}$$

Note that each $k(\Omega)$ relation found above contains the term $\cos(2\pi\Omega)$, so for any k there is an infinite number of modes at Ω, $1 - \Omega$, $1 + \Omega$, $2 - \Omega$, $2 + \Omega$ ..., the dispersion relations are periodic in Ω. Note also that at the G, X, and M points, analytic formulas for the mode frequencies, cut-off frequencies, are straightforward. Finally, it is also worth mentioning that the imaginary part of the wavenumbers can be obtained from the dispersion relation, and it is especially relevant in the band-gaps where the modes are evanescent. The analytical dispersion relations obtained above are plotted in Fig. S3.
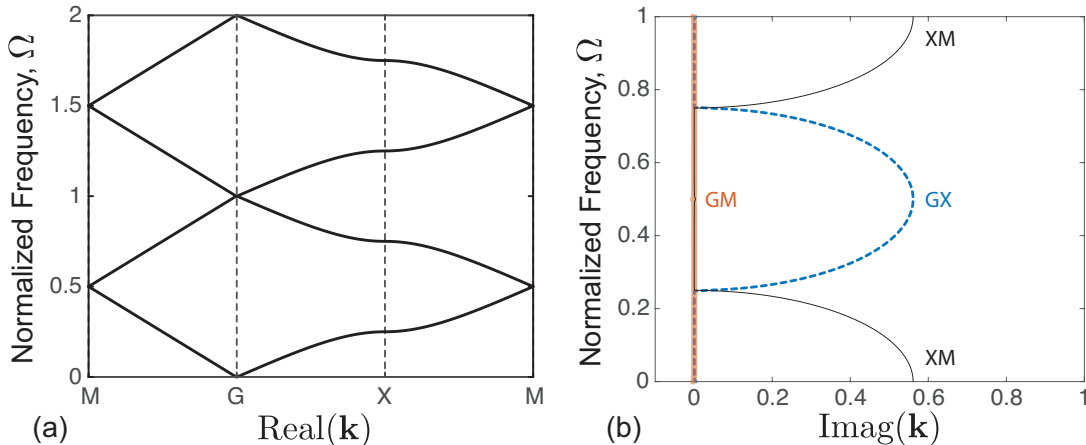

FIG. S3: Dispersion curves of the square network obtained from the analytical expressions (S12), (S14), (S16). (a) Normalized frequency as a function of Real($\mathbf{k}$), (b) Normalized frequency as a function of Imag($\mathbf{k}$).

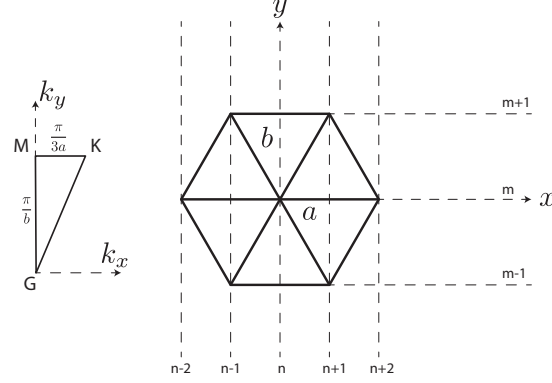**Dispersion relation for the triangular acoustic network ($N = 6$)**

FIG. S4: Geometrical configuration of the triangular lattice and Brillouin zone definition.

For the triangular acoustic network we have $N = 6$, so that Eq. (S5) becomes

$$6p\cos(2\pi\Omega) - \sum_{i=1}^{6} p_i = 0. \tag{S17}$$

Focusing on the junction labelled with the indexes (m, n) in Fig. S4, Eq.(S17) can be rewritten as

$$6p\cos(2\pi\Omega) - p_{(m,n+2)} - p_{(m+1,n+1)} - p_{(m+1,n-1)} - p_{(m,n-2)} - p_{(m-1,n-1)} - p_{(m-1,n+1)} = 0. \tag{S18}$$

Assuming periodicity and a solution in the form of a propagating wave $e^{-\imath ak_x x - \imath bk_y y}$, with k_x and k_y the coordinates of the wave vector $\mathbf{k}$, $a = L/2$, $b = L\sqrt{3}/2$, we obtain,

$$6\cos(2\pi\Omega) - e^{-2\imath ak_x} - e^{2\imath ak_x} - e^{\imath ak_x - \imath bk_y} - e^{-\imath ak_x + \imath bk_y} - e^{-\imath ak_x - \imath bk_y} - e^{\imath ak_x + \imath bk_y} = 0, \tag{S19}$$

which can be simplified into,

$$6\cos(2\pi\Omega) - 2\cos(2ak_x) - 4\cos(ak_x)\cos(bk_y) = 0. \tag{S20}$$

To construct the dispersion diagram for the triangular acoustic network we solve the dispersion equation Eq. (S20) on the GKM contour shown in Fig. S5. For the GM branch, we have $k_x = 0$ and $k^{GM} = bk_y \in [0, \pi]$. Therefore, Eq. (S20) simplifies into,

$$k^{GM} = \arccos(3\cos(2\pi\Omega)/2 - 1/2), \tag{S21}$$

which can be inverted, yielding

$$\Omega = \frac{1}{2\pi}\arccos[2\cos(k_{GM})/3 + 1/3]. \tag{S22}$$

For the GK branch, we have $k_y = 3k_x = k^{GK} \in [0, \pi]$ and Eq. (S20) simplifies into,

$$\Omega = \frac{1}{2\pi}\arccos[2\cos(2k^{GK}/3)/3 + \cos(4k^{GK}/3)/3]. \tag{S23}$$

Finally, for the KM branch we have $k_y = 2\pi/\sqrt{3}$ and $k_x = k^{GK} \in [0, \pi/3]$ and Eq. (S20) simplifies into,

$$\Omega = \frac{1}{2\pi}\arccos[\cos(2k^{KM})/3 - 2\cos(k^{KM})/3]. \tag{S24}$$

In point K $(2\pi/3, 2\pi/\sqrt{3})$, the band gap is of the smallest width, so it is interesting to obtain the associated frequency which determines the width of the complete band gap. For this, Eq. (S26) can be taken at $k^{GK} = \pi$, and it gives,

$$\Omega_K = \frac{1}{2\pi}\arccos[2\cos(2\pi/3)/3 + \cos(4\pi/3)/3], \tag{S25}$$

$$\Omega_K = \frac{\arccos[-1/2]}{2\pi} = 1/3. \tag{S26}$$

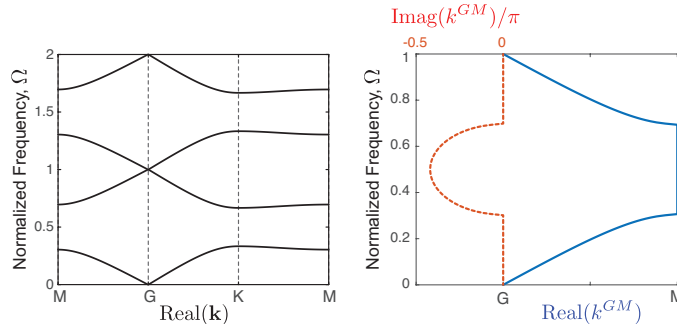The width of the band gap is consequently $1 - \Omega_K - \Omega_K = 1/3$.

FIG. S5: Dispersion curves of the triangular network obtained from the analytical expressions (S22), (S26), (S24). (a) Normalized frequency as a function of Real($\mathbf{k}$), (b) Normalized frequency as a function of Imag(k^{GM})/π and Real(k^{GM}).

NUMERICAL CALCULATION OF DISPERSION RELATIONS FOR PERIODIC ACOUSTIC NETWORKS

Finite Element formulation

In this study we focus on acoustic networks comprising a periodic array of narrow air channels of length L and cross-sectional width D, for which $D << L$. Therefore, in any individual channel the free vibrations of the enclosed air column can be described by the 1D wave equation [1, 3]

$$\frac{\partial^2 p}{\partial t^2} - c^2 \frac{\partial^2 p}{\partial x^2} = 0, \tag{S27}$$

where p is the acoustic pressure (the local deviation from the ambient pressure), c is the speed of sound in the channel and $x \in [0, L]$ denotes the position along the channel. Since Eq. (S27) in the general case cannot be solved analytically for a any complex periodic network of air channels, we determine its solution numerically by using the finite element (FE) method.

To develop the FE formulation, we start by restating Eq. (S27) in the weak form. We multiply both terms in Eq. (S27) by an arbitrary function $w(x)$ and integrate over the domain $[0, L]$,

$$\int_0^L w \frac{\partial^2 p}{\partial t^2} dx - c^2 \int_0^L w \frac{\partial^2 p}{\partial x^2} dx = 0. \qquad \forall w. \tag{S28}$$

Using integration by parts

$$w \frac{\partial^2 p}{\partial x^2} = \frac{\partial}{\partial x}\left(w \frac{\partial p}{\partial x}\right) - \frac{\partial w}{\partial x}\frac{\partial p}{\partial x}, \tag{S29}$$

Eq. (S28) can be rewritten as

$$\int_0^L w \frac{\partial^2 p}{\partial t^2} dx - c^2 \left[\int_0^L \frac{\partial}{\partial x}\left(w \frac{\partial p}{\partial x}\right) dx - \int_0^L \frac{\partial w}{\partial x}\frac{\partial p}{\partial x} dx\right] = 0, \qquad \forall w, \tag{S30}$$

which, using the fundamental theorem of calculus, can be simplified to

$$\int_0^L w \frac{\partial^2 p}{\partial t^2} dx - c^2 \left[\left.w \frac{\partial p}{\partial x}\right|_\Gamma - \int_0^L \frac{\partial w}{\partial x}\frac{\partial p}{\partial x}\partial x\right] = 0, \qquad \forall w, \tag{S31}$$

where Γ is the boundary of the 1D channel and consists of the two end points. In the following, the portion of the boundary where the p is prescribed is denoted by Γ_p, while the boundary where $\partial p/\partial x$ is prescribed is denoted by $\Gamma_{\partial p}$. Note that $\Gamma_p \cup \Gamma_{\partial p} = \Gamma$ and $\Gamma_p \cap \Gamma_{\partial p} = 0$. Next, we construct the arbitrary function $w(x)$ so that $w = 0$ on Γ_p and the pressure field so that $p = \bar{p}$ on Γ_p, yielding

$$\int_0^L w \frac{\partial^2 p}{\partial t^2} dx - c^2 \left[w \frac{\partial p}{\partial x} \Big|_{\Gamma_{\partial p}} - \int_0^L \frac{\partial w}{\partial x} \frac{\partial p}{\partial x} \partial x \right] = 0, \qquad \forall w \text{ with } w = 0 \text{ on } \Gamma_p, \tag{S32}$$

To numerically solve Eq. (S32), we then construct a mesh, introduce an approximation for the scalar fields p and w and formulate the discrete FE equations. Here, we discretize the 1D air channels into a number of line elements of length L_e and choose to approximate the fields in each line as a linear function (so that each element has two nodes located at x_1^e and x_2^e). It follows that over each element p and $\partial^2 p/\partial t^2$ are approximated as

$$p^e(x) = \mathbf{N}^e(x)\mathbf{d}^e, \qquad \frac{\partial^2 p^e(x)}{\partial t^2} = \mathbf{N}^e(x)\ddot{\mathbf{d}}^e, \tag{S33}$$

where $\mathbf{d}^e$ and $\ddot{\mathbf{d}}^e$ are vectors containing the nodal values of p and $\partial^2 p/\partial t^2$ and

$$\mathbf{N}^e(x) = \frac{1}{L_e}[x_2^e - x, \ x - x_1^e] \tag{S34}$$

is the so-called element shape function matrix. Note that the superscript e has been introduced to indicate that the functions pertain to element e. Moreover, according to the Galerkin method, we use the same approximation also for w,

$$w^e(x) = \mathbf{N}^e(x)\mathbf{w}^e. \tag{S35}$$

Next, to efficiently integrate Eq. (S32), we evaluate the integral over $[0, L]$ as a sum of integrals over individual element domains $[x_1^e, x_2^e]$,

$$\sum_{e=1}^{n_{el}} \left\{ \int_{x_1^e}^{x_2^e} w^{eT} \frac{\partial^2 p^e}{\partial t^2} dx + c^2 \int_{x_1^e}^{x_2^e} \frac{dw^{eT}}{dx} \frac{dp^e}{dx} dx - c^2 \left(w^{eT} \frac{dp^e}{dx} \right)_{\Gamma_{\partial p}^e} \right\} = 0, \tag{S36}$$

where n_{el} is the total number of line element used to construct the mesh. Note that in the equation above we have taken the transpose of the arbitrary function w; this does not change the value of the expression as w is a scalar, but it is necessary for consistency when we substitute matrix expressions for w and its derivatives.

Substitution of Eqs. (S33) and (S35) into Eq. (S36) yields

$$\sum_{e=1}^{n_{el}} \mathbf{w}^{eT} \left\{ \underbrace{\int_{x_1^e}^{x_2^e} \mathbf{N}^{eT} \mathbf{N}^e dx}_{\mathbf{M}^e} \ddot{\mathbf{d}}^e + c^2 \underbrace{\int_{x_1^e}^{x_2^e} \mathbf{B}^{eT} \mathbf{B}^e dx}_{\mathbf{K}^e} \mathbf{d}^e - \underbrace{c^2 \left(\mathbf{N}^{eT} \frac{dp}{dx} \right)_{\Gamma_{\partial p}^e}}_{\mathbf{f}^e} \right\} = 0, \tag{S37}$$

where

$$\mathbf{B}^e = \frac{\partial \mathbf{N}^e}{\partial x} = \frac{1}{L_e}[-1, 1]. \tag{S38}$$

Note that in Eq. (S37) we have introduced the element matrices $\mathbf{M}^e$ and $\mathbf{K}^e$

$$\mathbf{M}^e = \int_{x_1^e}^{x_2^e} \mathbf{N}^{eT} \mathbf{N}^e dx = \frac{L_e}{6} \begin{bmatrix} 2 & 1 \\ 1 & 2 \end{bmatrix}, \qquad \mathbf{K}^e = c^2 \int_{x_1^e}^{x_2^e} \mathbf{B}^{eT} \mathbf{B}^e dx = \frac{c^2}{L_e} \begin{bmatrix} 1 & -1 \\ -1 & 1 \end{bmatrix}, \tag{S39}$$

and the element vector $\mathbf{f}^e$

$$\mathbf{f}^e = c^2 \left(\mathbf{N}^{eT} \frac{dp}{dx} \right)_{\Gamma_{\partial p}^e}, \tag{S40}$$

which are the essence of the FE method formulation for this problem and serve as the building block for its global implementation.

Since the element and global nodal vectors can be related as

$$\mathbf{d}^e = \mathbf{L}^e\mathbf{d}, \qquad \ddot{\mathbf{d}}^e = \mathbf{L}^e\ddot{\mathbf{d}}, \qquad \mathbf{w}^e = \mathbf{L}^e\mathbf{w}, \tag{S41}$$

where $\mathbf{L}^e$ is the gather matrix for a given element, which gathers the nodel quantities of each element from the global nodal vector (note that $\mathbf{L}^e$ is a Boolean and consists strictly of ones and zeros). Substituting Eq. (S41) into Eq. (S37) we obtain

$$\mathbf{w}^T \left(\sum_{e=1}^{n_{el}} \mathbf{L}^{eT}\mathbf{M}^e\mathbf{L}^e\ddot{\mathbf{d}} + \sum_{e=1}^{n_{el}} \mathbf{L}^{eT}\mathbf{K}^e\mathbf{L}^e\mathbf{d} - \sum_{e=1}^{n_{el}} \mathbf{L}^{eT}\mathbf{f}^e \right) = 0. \tag{S42}$$

If we now define the global matrices $\mathbf{M}$ and $\mathbf{K}$ as

$$\mathbf{M} = \sum_{e=1}^{n_{el}} \mathbf{L}^{eT}\mathbf{M}^e\mathbf{L}^e, \qquad \mathbf{K} = \sum_{e=1}^{n_{el}} \mathbf{L}^{eT}\mathbf{K}^e\mathbf{L}^e, \tag{S43}$$

and the global vector $\mathbf{f}$ as

$$\mathbf{f} = \sum_{e=1}^{n_{el}} \mathbf{L}^{eT}\mathbf{f}^e, \tag{S44}$$

Eq. (S42) can be rewritten as

$$\mathbf{w}^T \left(\mathbf{M}\ddot{\mathbf{d}} + \mathbf{K}\mathbf{d} - \mathbf{f} \right) = 0. \tag{S45}$$

Finally, since Eq. (S45) has to be satisfied of all possible $\mathbf{w}$, it follows that

$$\mathbf{M}\ddot{\mathbf{d}} + \mathbf{K}\mathbf{d} - \mathbf{f} = 0, \tag{S46}$$

which represent the FE equations for the 1D wave equation.

Frequency-domain analysis

To calculate the dispersion relation for an acoustic periodic network, we focus on its unit cell spanned by the lattice vectors $\mathbf{a}_1$ and $\mathbf{a}_2$ (highlighted in red in Fig. S6). We then consider the wave motion

$$\mathbf{d} = \mathbf{p}e^{\imath\omega t}, \tag{S47}$$

where $\mathbf{p}$ is the vector of nodal amplitudes of vibration and ω is the circular frequency. Introducing Eq. (S47) into Eq. (S46) we have

$$(\mathbf{K} - \omega^2\mathbf{M})\mathbf{p} = \mathbf{0}, \tag{S48}$$

which is a generalized eigenvalue problem. Note that here we consider a unit cell in isolation from other unit cells, and thus the global vector $\mathbf{f}$ has been set to zero.

Next, we apply Bloch-type boundary conditions, so that the pressure of each pair of nodes (here denoted as A and B) periodically located on the boundary of the unit cell is related as

$$\mathbf{p}_B = \mathbf{p}_A \exp(\imath\mathbf{k} \cdot \mathbf{r}_{AB}), \tag{S49}$$

where $\mathbf{k}$ is Bloch-wave vector and $\mathbf{r}_{AB}$ is the distance between the pair of nodes periodically located on the boundary.

Finally, we solve Eq. (S48) with (S49) for a number wave vectors $\mathbf{k}$ lying in the reciprocal space. Note that, since the reciprocal lattice is also periodic, we can restrict the wave vectors $\mathbf{k}$ to a certain region of the reciprocal space called the *first Brillouin zone* (indicated by the dashed polygons in Fig. S6). In addition, we may further reduce the domain to the *irreducible Brillouin zone* (IBZ) (indicated by the yellow areas in Fig. S6) by taking advantage of reflectional and rotational symmetries. Operationally, the band structures for the acoustic networks are constructed by calculating the eigen-frequencies $\omega(\mathbf{k})$ for $\mathbf{k}$ vectors on the perimeter of the IBZ and the band gaps (defined as frequencies range in which the propagation of the waves is forbidden) are obtained by the frequency ranges within no $\omega(\mathbf{k})$ exist. Numerically, a discrete set of $\mathbf{k}$ vectors on the perimeter of the IBZ needs to be chosen for the band gap calculations. For the simulations presented in this paper, twenty uniformly-spaced points on each edge of the IBZ are considered.

Dispersion relations for acoustic networks

While in Fig. 2 of the main text we report the dispersion curves for square and triangular lattices, we have also investigated the wave propagation in a number of other acoustic networks. In particular, in Fig. S6 we report the dispersion relations for Kagome (see Fig. S6(a)), hexagonal (see Fig. S6(b)), equilateral pentagonal (see Fig. S6(c)), mixed pentagons and rhombi (see Fig. S6(d)) and snub square (see Fig. S6(e)) configurations. Interestingly, the results indicate that any lattice comprising triangles or pentagons is characterized by frustration induced acoustic band gaps in the vicinity of the odd numbered resonance frequencies for the individual channels.
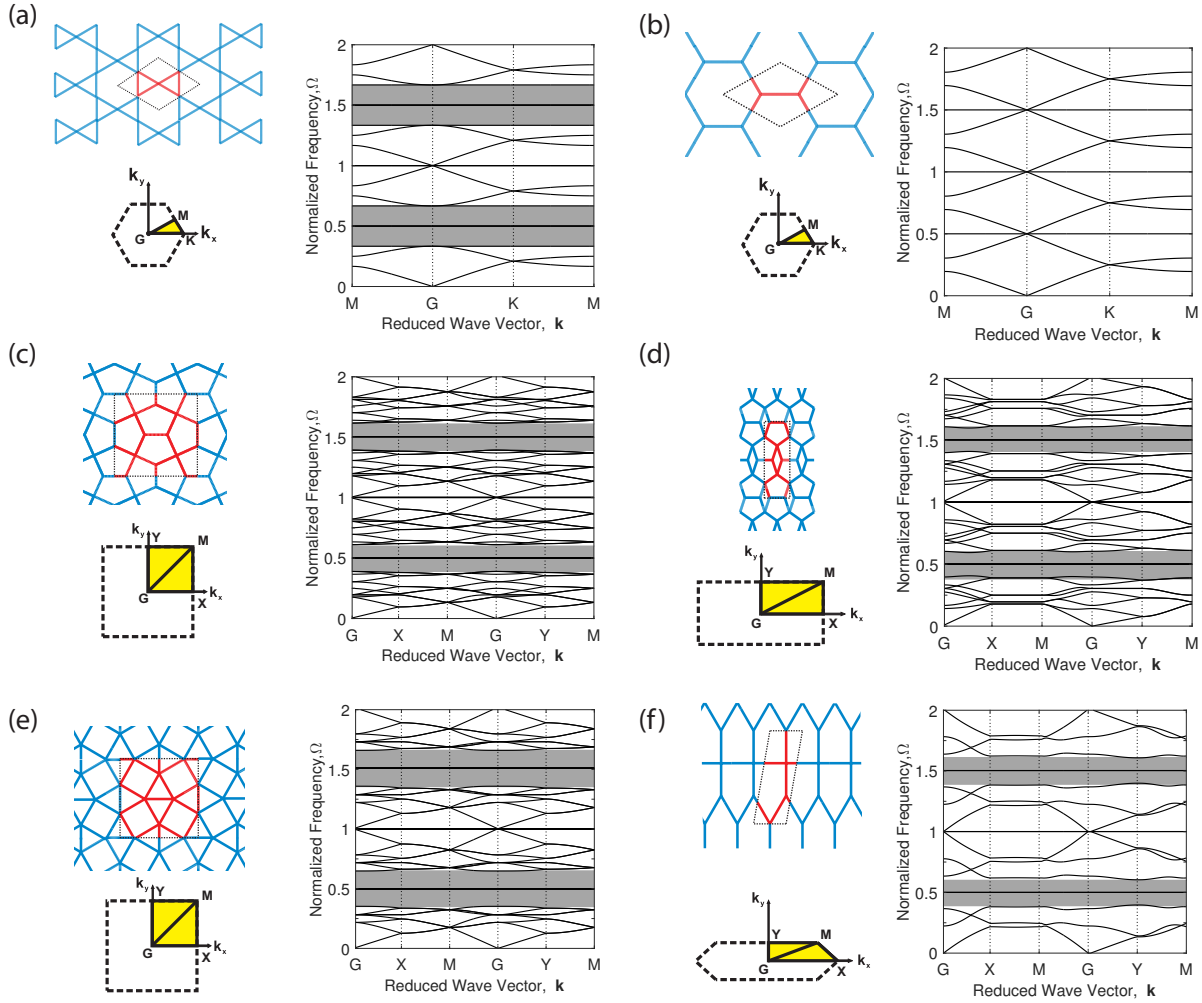

FIG. S6: Dispersion curves for acoustic networks comprising a periodic array of narrow air channels: (a) Kagome, (b) hexagonal, (c) equilateral pentagonal, (d) mixed pentagons and rhombi and (e) snub square lattices. Lattice configurations, unit cells (highlighted in red) and Brillioun zones are shown on the left. The calculated dispersion relations are shown on the right. The grey regions in the plots highlight the full band gaps induced by geometric frustration.

EFFECT OF THE FINITE WIDTH OF THE AIR CHANNELS

While the results presented in Fig. 2 of the main text are for ideal acoustic networks made of 1D channels, we have also investigated the effect of the finite width t of the tubes. To this end, we have performed FE simulations using the commercial package ABAQUS/Standard and studied the dynamic response of lattices comprising 2D rectangular channels of length L and width D meshed with 4-node bilinear acoustic elements (ABAQUS element type AC2D4). The calculated band structures for the square and triangular networks comprising channels with different values of L/D are reported in Figs. S7 and show that the dynamic response of the system is not significantly affected by the finite-width of the channels especially in the lower frequencies of the spectrum. Note that the even for the highest presented frequencies and the smallest ratio $L/D = 10$, only a single plane wave mode propagates in the individual channels. Thus the one-dimensional equation (S27) is still valid for describing the wave propagation in the individual channels. However the continuity condition at the junction Eq. (S4), derived for a wavelength much larger than the junction size, may not be valid anymore, and the actual scattering by the junctions may deviate from the long wavelength scattering. As a consequence, we observe in the numerical results that the flat, zero group velocity, standing wave modes are modified into slowly propagating modes when the ratio L/D is decreased.
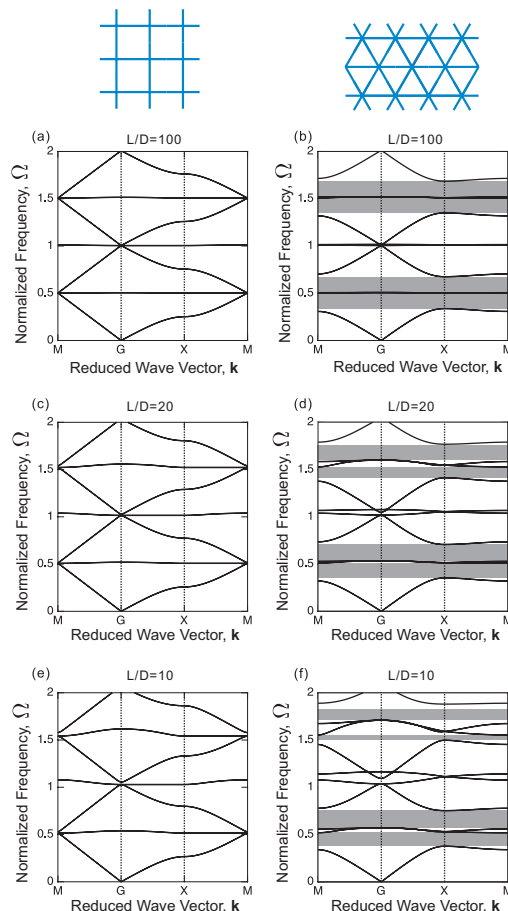

FIG. S7: Effect of the finite width D of the channels: band structures for the square and triangular networks characterized by different values of L/D. The grey regions in the plots highlight the full band gaps induced by geometric frustration.

[1] M. Bruneau and T. Scelo, *Fundamentals of Acoustics* (ISTE, UK and USA, 2006).
[2] C. Depollier, J. Kergomard, and Lesueur J.C., J. of Sound Vib. **142**, 153 (1990).
[3] P. M. Morse and K. U. Ingard, *Theoretical acoustics* (Princeton university press, 1968).